Application of image based measurement techniques for the investigation of aeroengine performance on a commercial aircraft in ground operation

A. Schröder[1,*], R. Geisler[1], D. Schanz[1], J. Agocs[1], D. Pallek[1]
M. Schroll[2,*], J. Klinner[2], M. Beversdorff[2], M. Voges[2], C. Willert[2]

1: Institute of Aerodynamics and Flow Technology, German Aerospace Center (DLR), 37073 Göttingen, Germany
2: Institute of Propulsion Technology, German Aerospace Center (DLR), 51170 Köln, Germany
* correspondent authors: Andreas.Schroeder@dlr.de, Michael.Schroll@dlr.de

Abstract The investigation of the flow and sound field upstream and downstream of a full scale aeroengine is aimed at providing important reference data required for reliable modeling and prediction. In this regard a wide variety of contactless and non-invasive laser optical and acoustic measurement techniques have matured in recent years to allow their application on full scale aircraft. Within a measurement campaign involving an Airbus A320 DLR research aircraft inside a sound-attenuating hangar at Hamburg Airport, four image-based measurement techniques were applied in parallel to acquire data for the engine operating at varying conditions: stereoscopic PIV of the engine intake and jet exhaust flow, high frame rate BOS of the exhaust jet in combination with acoustic array measurements, IPCT/PROPAC technique for the measurement of fan blade deformation under load and MODE measurements for nacelle position monitoring. The objective of the ground tests was to establish a combined measurement data base to locate the zones within the engine jet exhaust flow where large, turbulent fluctuations in velocity and density produce noise. Simultaneous application of PIV, BOS and acoustic array techniques were carried out in front and behind the left aircraft jet engine, for the characterization of inlet flow disturbance due to ground vortex formation, the turbulent free jet flow field as well as engine's core and jet noise. The installed ground test instrumentation was operated in parallel to facilitate a simultaneous acquisition of various flow field parameters using different diagnostic approaches (instantaneous velocity, sound pressure and fluctuation, density fluctuations and fan blade deformation). The diagnostics were applied non-invasively to the aircraft and aeroengine, that is, the ground test hardware neither required modifications to the aircraft airframe or engines nor had any direct connection to the aircraft which significantly eased the certification and test approval procedure. Nonetheless parts of the test equipment had to be installed within the danger (safety) area of the engines and required numerous certification and approval steps. The paper focuses on the implementation and use of the laser optical measurement techniques PIV and BOS in this challenging, full scale application.

1. Introduction

The motivation of the DLR project SAMURAI – "Synergy of Advanced Measurement techniques for Unsteady and high Reynolds number Aerodynamic Investigations" – is driven by an important goal addressed in the ACARE[1] Vision 2020: the reduction of noise- and exhaust-emissions for air traffic in the near future. This reduction can only be achieved by technical improvements, which require an improved knowledge of the basic physical processes, in particular related to aircraft engine flows and in the aerodynamics of wings in high-lift-configurations. For the understanding of these intrinsically unsteady high Reynolds number flows (flow separation, transition, turbulence, vortex development and dynamics) and related flow-structure-interaction and flow induced noise sources imaged based measurement methods are an indispensable tool for the determination of fluid mechanical significant measures in whole fields and on surfaces of (model-) parts in the flow. Nowadays, numerical methods have matured to a degree that allow prediction of unsteady and high Reynolds number aerodynamics by applying adapted turbulence- and transition-models or advanced simulation methods. In order to qualify these simulation tools for the design process of innovative aircraft concepts requires a coupling of these CFD codes with CSM and CAA methods for an integrated approach one the one hand. Of equal significance are extensive validation experiments using image based measurement methods are, because they have the capability of providing (unsteady) measurement data in fields and volumes [1] at sufficiently high spatial and temporal resolution.

[1] All used abbreviations are listed at the end of the paper

Over past two decades the DLR institutes of "Aerodynamics and Flow Technology" and "Propulsion Technology" have developed a variety of complementary non-intrusive, image based measurement techniques (PIV, BOS, PROPAC, IPCT, MODE, Acoustic Array, PSP, TSP, IRT) for mobile use in wind tunnels and free flight experiments. In the course of these developments considerable knowledge has been accumulated in applying these measurement techniques for the aerodynamic, aeroacoustic and aeroelastic characterization of wind tunnel models. The combined application of optical and acoustic measurement techniques enables the quantification of different fluid mechanically, aero-acoustically and -elastically relevant measurement categories like pressure, velocity vectors, density, model deformation and noise sources in fields, on surfaces or even in whole. Even unsteady field data can be achieved that previously were unattainable. Such measurement data are of high importance for the development, validation and combination of complex simulation tools, like CFD (URANS, DES, LES, DNS), CSM or CAA. Furthermore, the combined application of these measurement techniques enables (partly for the first time) the investigation of physical interdependencies (e.g. the noise source mechanisms of vortical flows or the elastic effects of (dynamic) forces and moments on model parts) [1].

Derived from these requirements the superordinate goal of SAMURAI is to achieve a large field-dataset for the extension of the aerodynamic, aero-elastic and aero-acoustic knowledge of these complex flow regimes and for the validation of and combination with accompanying advanced numerical simulations. Because of that for two subordinated but central experimental fields of aerodynamic investigation combined image-based experimental measurement systems have been applied within the project SAMURAI: first, the high-lift-configuration wing represented by the F16-model and the "community friendly aircraft (BNF)" model and secondly jet engine flows, represented by the UHBR and the IAE V2527 engine of the A320 Aircraft. Basis for the present contribution is the experimental part of full scale jet engine flow on the A320-ATRA DLR research aircraft. The experiments were performed on the ATRA Aircraft during a week-long measurement campaign in September 2013 inside a sound-attenuating hangar of Lufthansa Technik at Hamburg Airport (Fig. 1). Within this measurement campaign four image-based measurement techniques were applied in parallel to acquire data from the IAE V2527 engine operating at conditions varying between idle and take-off:

- Stereoscopic PIV at the engine intake and engine jet exhaust flow, the latter in combination with acoustic array measurements
- High frame rate BOS at the exhaust jet in combination with acoustic array measurements
- IPCT and PROPAC technique for the measurement of fan blade deformation under load
- MODE measurements to obtain nacelle's reference position during the engine runs

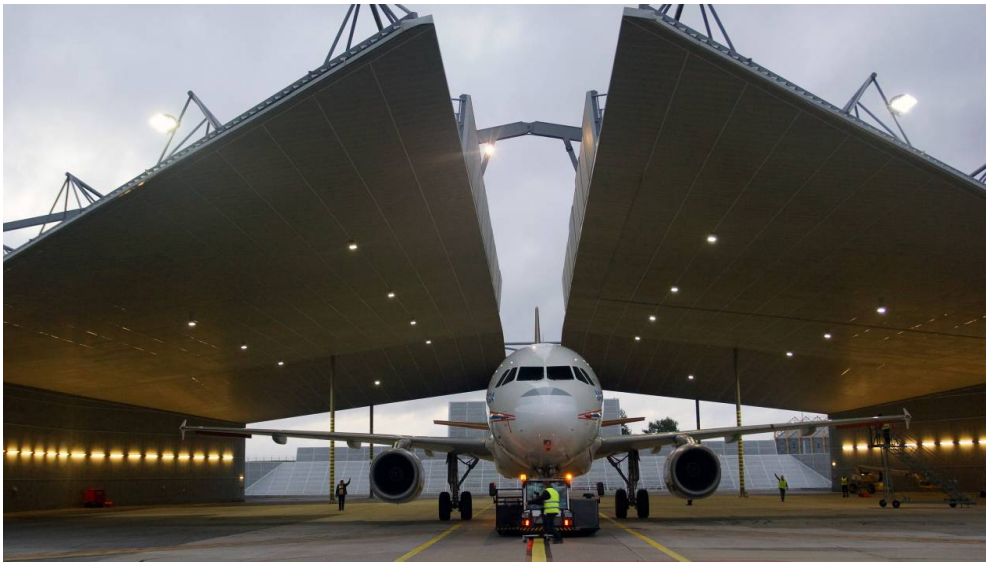

Figure 1: DLR's Advanced Technology Research Aircraft ATRA-A320 in the Lufthansa Technik sound-attenuating hangar at Hamburg Airport [2]

One main focus of these ground tests was the investigation of the noise production. Therefore the objective was to establish a combined measurement data base to locate the zones within the engine where large,

turbulent fluctuations in velocity and density produce noise. As shown in figure 2 simultaneous application of PIV (2,3), BOS (5) and acoustic array (6) techniques were carried out in front and behind the aircraft jet engine, for the characterization of inlet flow disturbance due to ground vortex formation, the turbulent free jet flow field as well as engine's core and jet noise. Furthermore the IPCT and PROPAC (1) techniques were applied to determine the fan blade deformation and vibration. MODE (4) measurements were used to monitor the shift of the nacelle caused by the tilt movement of the aircraft during the engine runs. For safety reasons, all measurement equipment installed inside the hangar had to be remote controlled. The acquired data serves as a basis for validation of numerical simulations that aim at predicting engine performance and noise emission. Due to the broad range of activities and results related to the measurement campaign, this contribution will focus on the implementation and use of the laser optical measurement techniques PIV and BOS in this challenging, full scale application.

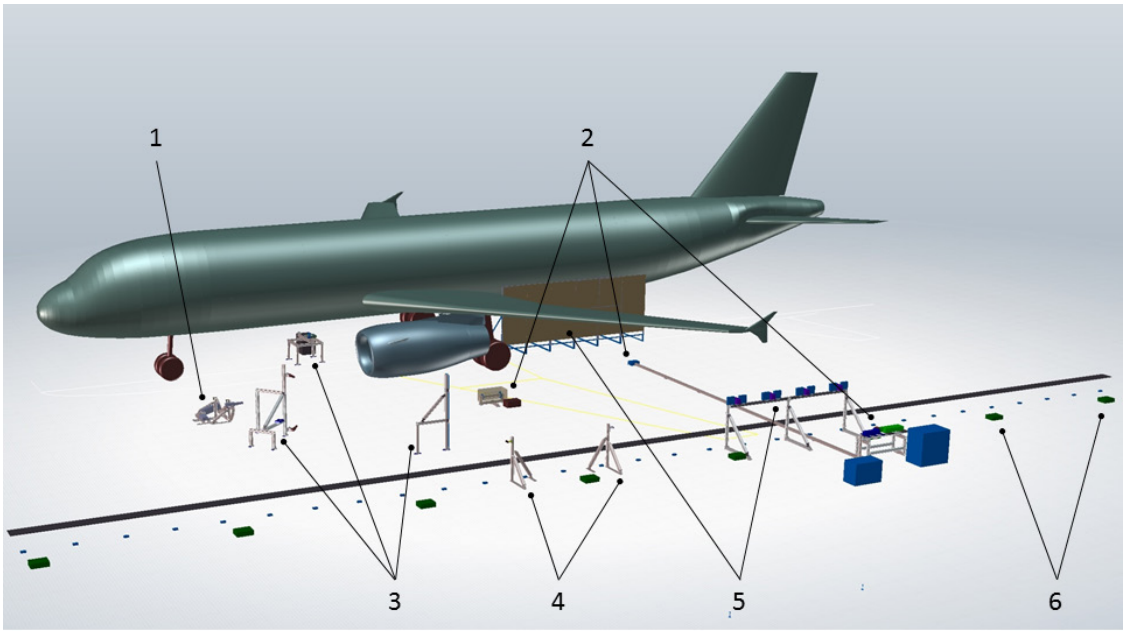

Figure 2: Complete measurement set up of IPCT/PROPAC (1), two SPIV systems for jet (2) and intake flow (3), MODE (4), BOS (5) and acoustic array (6) in order to observe the left IAE-V2527 engine of DLR's Advanced Technology Research Aircraft ATRA-A320

2. Specifications of Test Facility, Aircraft and Operating Conditions

The wide variety of delicate measurement equipment used for this week-long measurement campaign must remain installed inside a partially open hangar for several days, with the possibility of rainy conditions and cool and humid nights. During setup and ground testing stable and dry weather conditions are a requirement as heavy rain or/and strong wind will have adverse effects on the ground test equipment and the experiments on the whole. Based on long-time weather records the months of September and May were considered favorable in combination with early sunset ensuring sufficient time slots without daylight for PIV measurements in the late evening hours. Given both the predominant weather conditions in Germany as well as the lack of airports in sparsely populated areas with sufficient technical support it was necessary to find a suitable hangar without disturbing the residents of nearby towns during the engine runs. The choice fell quickly to Europe's largest and almost fully enclosed soundproof hangar in Hamburg which has been in operation since 2002 for engine tests for all airplanes serviced by Lufthansa Technik (LHT, German maintenance, repair and overhaul suppliers. The soundproof hangar in Hamburg - a model for similar facilities in Leipzig, Zurich and Geneva - was constructed on the initiative of Flughafen Hamburg GmbH and is the first closed soundproof hangar, world-wide. Conducting their own microphone measurements outside the hangar during the foreseeable and therefore predictable week-long test series, the operators were able to acquire additional data on the soundproofing performance of the building [2].

The hangar measures 95 by 92 meters beneath a 23-meter high roof and can accommodate a Boing 747-800 aircraft (Fig. 3). For engine test runs, the aircrafts are pushed backward into the hangar, which is then closed by two each 56-meter-wide and 300-ton gates [3] that essentially are comprised of large scale tuning vanes with acoustically dampened surfaces (Fig. 3, left). The gap in the ceiling for the aircraft fin is sealed by flaps

after parking the aircraft, which for the present application offered additional protection of the measurement equipment located under the aircraft fuselage. To facilitate sufficient airflow the hangar can never be completely closed and offers a working environment that is far from laboratory conditions. Therefore it was necessary to package essentially all measurement instrumentation inside protective housings including temperature control. Given that ground testing inside the hangar generally is self-sustained, that is, the engines run on their own power and require no external supply, the facility only provides minimal infrastructure required for the operation of laser-optical measurement systems. It was necessary to supply water for laser cooling from a nearby fire hydrant and compressed air for the aerosol seeder from an external mobile compressor, while sufficient electrical support was already available. Outside the hangar four shipping containers served as control rooms, stock room as well as social room.

Figure 3: Sound-attenuating hangar at Hamburg Airport (left), a B747-800 inside the hangar (right) [3]

The test object for the SAMURAI measurement campaign is DLR's "Advanced Technology Research Aircraft (ATRA), an Airbus A320 MSN 659 equipped with two IAE-V2527 engines (Fig. 1). For this ground test campaign the allocation of the ATRA consisted of 7 days of use with engine operation of up to 10 hours in 4 cycles (run up – run down) including 19 cycles at maximum continuous thrust (MCT, aircraft on brakes) and a final cycle idle- MCT -TOGA (Take-off-go-around). The dimensions of the ATRA are:

- fuselage: length 37.57 m, height ~6 m, ground clearance 1.82 m
- wing span 34.1 m,
- fin height fin 11.76 m
- engine: height 1.8 m (core plug), diameter 1.8 m, inlet inclination 6°, ground clearance 0.85 m, inlet distance from nose 11 m

Once the ground test equipment is installed the aircraft cannot leave the test facility as this would require dismantling a large amount of the instrumentation. For the scope of jet noise measurements some meteorological requirements need to be observed that are based on the definitions of the ICAO Annex 16 and the Environmental Technical Manual on aircraft noise measurements: :

- precipitation (heavy rain, dust, snow, dew)
- relative humidity higher than 80% or lower than 20%
- ambient temperature above 35°C or below 10°C
- reported wind above 19 km/h (10 kts) or cross wind above 9 km/h (5 kts), using a 30 s average

The unpredictability of weather conditions may in fact result in delay in the test schedule such that several alternative time slots for measurement runs were defined a priori.

3. Certifications (FTR, laser safety regulations, DEHS)

Any measurements involving an aircraft in flight or even ground tests necessitates an extensive (in time and amount) documentation called Flight Test Request (FTR), listing the aircraft configuration, the test equipment, the required FTI configuration and requested result forms, a description of test and test area, a test program and schedule in smallest detail and possible limitation. For the present SAMURAI test campaign it additionally includes laser safety regulations. During the ground test PIV lasers of laser class 4 needed to be operated for which strict laser safety restrictions applied. The flight crew on board was protected from possible laser reflections and diffuse stray light by laser safety goggles and by partially closed

window shades in the cabin. Access to the hangar was only permitted using the control room entrance and exit doors. The entire hangar and surrounding area had to be treated as laser safety area and was protected by warning lights, signs or access barriers. Only trained specialists of DLR ground test crew were allowed into the laser safety zones during laser operation. Access to the hangar through the open emergency exit at the back end of the hangar or through the guide vanes of the hangar doors was strictly forbidden. Due to the gap between hangar roof and exhaust deflection vane at the rear end of the hangar the airport tower had visual access into the hangar and the instrumentation installed inside. This permitted a direct view of the diffuse laser reflection on the engine core plug caused by the laser light sheet needed for SPIV in the jet flow (Fig. 4). Given that the air-traffic-controllers use binoculars posed a potential laser hazard, especially during the night time when the PIV measurements were to be performed. Furthermore diffuse laser reflections could not be completely prevented from being visible outside of the hangar and pose the risk of irritation of nearby pilots. Because of the rather short distance to the tower of ~450 m (Fig. 5) each PIV run had to be coordinated with air-traffic-control during ongoing airport operations and required a single clearance during the night shift. In the laser safety documentation the critical distance to the core plug laser reflection while using typically binoculars (7x50 magnification) was determined to 350 m at daylight conditions, about 100 m below the given distance [4]. During the actual measurement campaign the air traffic controllers confirmed no noticeable impairment due to the laser reflections, neither at day time nor at night.

Figure 4: Laser light sheet from behind engine hitting the core plug with diffuse reflection

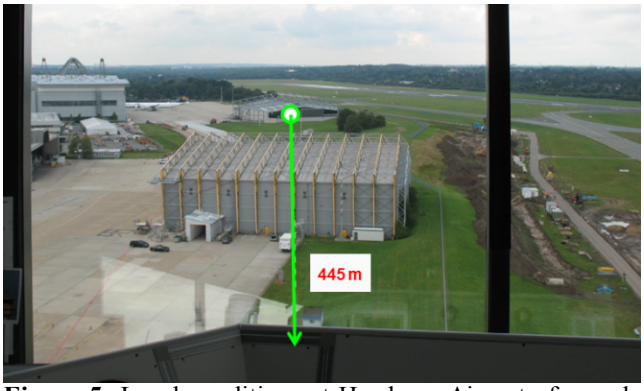

Figure 5: Local conditions at Hamburg Airport of sound-attenuating hangar and tower with direct view line

Inherent to the PIV measurement technique is a sufficient amount of homogeneously distributed µm-sized particles within the field of view. For the present application atomized DEHS was chosen to seed the engine inlet duct and the flow downstream of the engine. The use of the seeding material required approval by the IAE consortium. During engine operation the majority of particles is expected to move through the bypass section, which is desired in order to enable SPIV measurements in the exhaust jet. The risk for engine parts was rated to be low, but as a certain amount of particles passes through the core engine, an engine wash procedure was deemed necessary after the ground test campaign according to aircraft maintenance and flight safety procedures. Ultimately only a small residue in the region of the inlet lip was established after the completion of the measurements. No residue could be found on either the fan or in the outlet nozzle region.

During the prior acoustic measurements on ATRA within SAMURAI performed in May 2013 considerable oscillations were observed stabilizer and vertical fin, which are attributed to interaction of the engine exhaust jet with the aircraft and ground. These oscillations were particularly significant during ground tests at higher operating conditions like MCT. Within the “A320 AMM High Power Assurance Test” manual ground test above 75% of fan speed (N1) are limited to 2 minutes and requires 3 min stabilization at 75% in advance and a subsequent 5 min cooling down at idle conditions. This regulation significantly restricted the maximum amount of data at MCT for all image acquisition systems at each run being limited by camera or laser frequencies compared to initial planning. Additionally it was decided to monitor the aircraft accelerations during the long term ground test measurements in Hamburg by an array of acceleration sensors installed on horizontal and vertical stabilizers [4].

The engine ground tests were performed at maximum continuous thrust (MCT), which corresponds to the maximum possible thrust for the ATRA on brakes and corresponds to ~82% fan speed N1. At MCT engines produce a considerable thrust, which leads to a considerable forward shift and slight lean of the entire aircraft

even on brakes due to overall flexibility of the airframe structure and deformation wheel suspension. In addition forces and moments from the engine on the wing cause movement of the nacelle relative to the aircraft. Finally even nacelle's height about ground changes in the course of the runs due to changing fuel load. In order to put the results obtained later in relation with an engine coordinate system, all optical measurement techniques require a reference to the engine at MCT, but can only be set at engine stop. Because of this restriction nacelle's position had to be monitored during the runs to ensure subsequent determination of the measurement planes in respect to nacelle all items (cameras, target, and nacelle) had to be determined in a common global coordinate system.

Figure 6 shows the danger areas of the ATRA-A320 at take-off thrust which are comparable to the investigated MCT. For stable aircraft operation on ground, the thrust levers for both engines have to be in the same position, with aircraft on brakes. Because of extensive equipment installed very close to the danger (intake) zone in front of the aircraft engine and the BOS wall very close to the fuselage a video documentation with two cameras during the engine runs was required. For every item installed around the aircraft like frames, supports and even the cable bridges on the floor the expected wind load was calculated. Suitability of the ground fixtures had to be confirmed by tensile tests before the measurements. Adhesive tapes, markers or adhesives all required an aviation authorization.

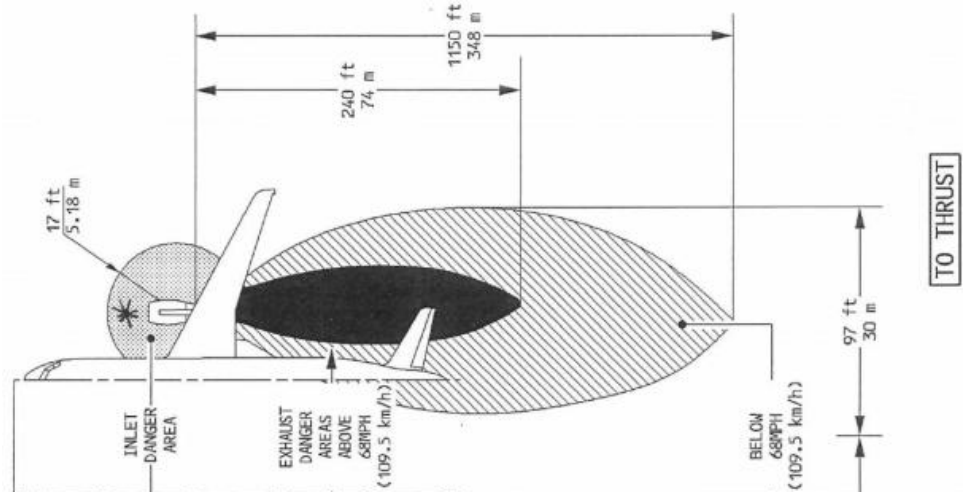

Figure 6: Danger areas of the ATRA-A320 at take-off thrust

4. MODE Setup and 1/Ref signal

Monitoring the engine movement was performed by marker-based optical deformation examination (MODE) as shown in figure 7. The setup consists essentially of checker board markers (removable adhesive foil) applied on the nacelle, a powerful LED lamp for illumination during PIV runs in the dark, two CCD cameras (AVT GX3300) and a corresponding data acquisition computer system. Cameras, lamp supports and computer rack are placed in a position orthogonal to nacelle, 18 m outboard from centerline (17 m half wing span). Aim of the measurement technique is the determination of the position of the common reference point "core plug" (per definition) based on a marker-based photogrammetric evaluation during the test runs. Because this reference point on the core plug is obscured from view by the MODE system its position must be inferred from the evaluation of the marker positions that are applied to the nacelle (Fig. 8). The change in position regarding a reference image is determined in the camera coordinate system. The nacelle is assumed to be an ideal rigid body. Under this condition, the determined change in position in the camera system can be applied to the reference points. For the measurement techniques in addition to the location of the reference point, the angle to the engine axis are relevant. The engine axis is approximated by the two points spinner tip and core plug. Finally the position of the reference point "core" and the spinner, as well as the position of PIV and BOS systems and their calibration targets are measured within the world coordinate system by a tachymeter at engine stop condition. Based on this data the relative position of the measurement planes with respect to nacelle are determined afterwards. The average nacelle offset shift is about 100 mm for MCT in forward direction.

For rotation angle correlated IPCT/PROPAC measurements at the fan it is necessary to operate a 1/rev signal

transmitter based on N1 rpm of the investigated left engine 1, connected to the DLR equipment outside of the aircraft. This signal is required to synchronize and trigger the measurements to a fixed fan blade phase angle. The signal supply/transmitter unit was provided and installed by LHT, well experienced with the V2527 engine.

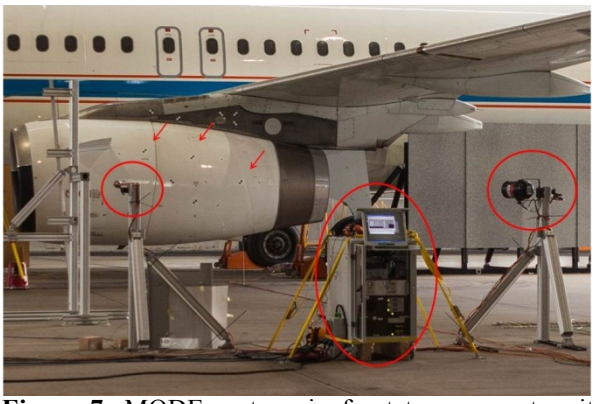

Figure 7: MODE system; in front two supports with cams and LED lamp (circles), DAQ centered (ellipse); in background: nacelle with reference markers (arrows)

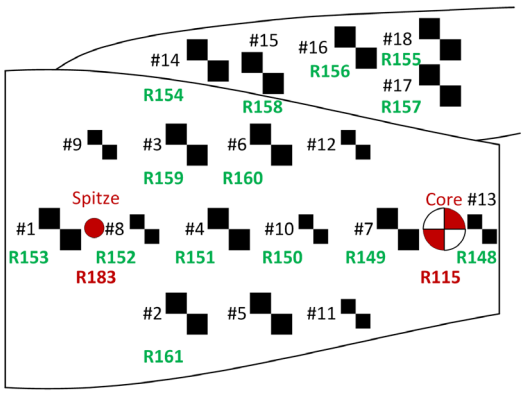

Figure 8: Reference markers on nacelle in reference to core plug as chosen relative coordinate origin

5. PIV Setup for Inlet Flow

The stereoscopic PIV setup in front of the engine as shown in figure 9 was dedicated to investigate the inlet flow of the V2527 engine, which can be influenced by the formation of ground vortex structures.

Operation of the measurement equipment was completely managed and monitored from a control room, located in container offices outside of the hangar (Fig. 11). For all measurement techniques involved in the ground tests, the corresponding components were assembled in the laboratory based on mock-ups or realistic 1:1 replicas to verify the feasibility of each system. These included for example the design of the magnification scale in relation to possible camera CCD dimensions and corresponding lenses (including focal length, field of view distances). Finally all components needed to be certified within the tensile test requirements for FTR approval.

The inlet flow in front of the engine was examined by a stereoscopic PIV system consisting of a laser type Brilliant B Quantel, 2x 320 mJ @10 Hz; two 2 PIV cameras type PCO.2000, ROI 2048 x 2048 pixel, 7.49 Hz @fullROI (PCO AG); two Scheimpflug camera mounts; two RAID storage computers and one remote computer; a timing controller (ILA GmbH); light sheet optics and a beam dump. The size of the measurement domain was approximately 1100 x 400 mm² in a cross section of the intake flow in radial and stream-wise direction. The mean horizontal magnification factor of both cameras is about M = 1.7 px/mm, in vertical direction about 2.3 px/mm. Final alignment of the stereo viewing has been achieved with sub-pixel accuracy using the disparity correction scheme on the mapped particle images implemented in PivView3.59.

Figure 9: PIV system with laser in the back (circle); cameras in casings in front (arrows); aluminum boxes as electronic safety boxes (ellipses)

Figure 10: Laser under fuselage with outboard directed light sheet in front of the blackened engine inlet lip

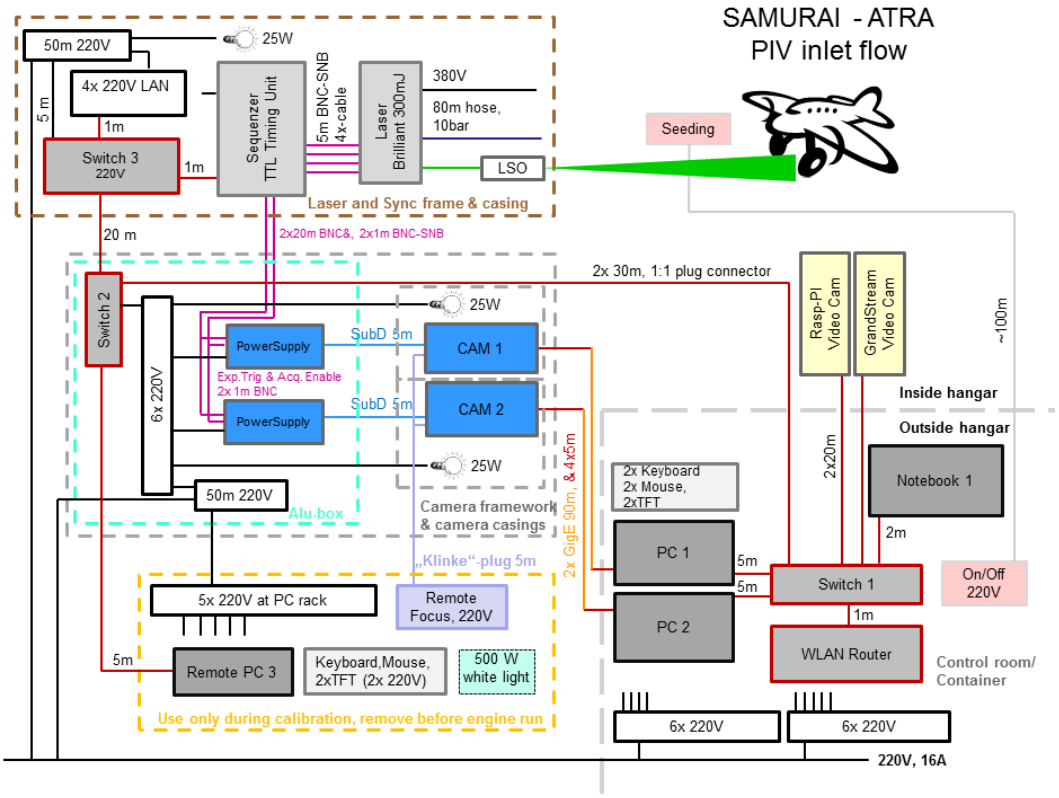

Figure 11: Cable plan of remote controlled PIV setup for inlet flow at ATRA

The laser with its power supply was located near the aircraft centerline underneath the fuselage, with beam height 1.25 m above ground level. The laser was mounted on a rigid aluminum frame (Linos X95) with light sheet optic directly in front of the laser head, visible in the back of figure 9. The light sheet was positioned a few centimeters upstream of the engine intake plane (with respect to engine load conditions). Because laser radiation was directed to hangar's main control room a beam dump had to block the laser light sheet. The sequencer was placed in a sealed aluminum box next to the laser to protect cable connectors, sockets and LAN switch. Cameras and their power supplies were protected in a similar manner. The PIV system was configured to operate at laser flash lamps at 10 Hz with cameras and Q-switches triggered at 5 Hz. The laser pulse separation was set to 20 µs. Both cameras were mounted on a Scheimpflug adapter supporting remote controlled focus for the used Zeiss macro-planar lenses ZF 2/100 with chosen aperture of $f_{\#} = 5.6$. The cameras had to be enclosed in a casing to avoid the risk of any small parts loosened by vibration from flying into the engine. These casings are mounted on a X95-frame, located 4 m outboard and 4.5 m upstream the engine, just outside the ultimate danger zone of 5.18 m (Fig. 6), with an inclination angle of 45° regarding engine axis. While the position of camera is close to ground level, the second camera is positioned at a height of 2.4 m. GigE interface was used for image data transfer with each camera connect directly connection to a RAID computer at external control room (100 m cabling).

For calibration, which definitely needed to be done inside the hangar close to the camera and light sheet, a third mobile computer was used, integrating both RAID units as remote desktop session on separate screens. This third computer had to be removed before every engine run. Calibration was performed on a target with checker board with 100 x 100 mm² squares placed on a support observing the inclination angle of 6° corresponding to the inlet geometry (Fig. 12). The light sheet was arranged 200 mm upstream the inlet to ensure a measurement plane distance of about 100 mm after the nacelle offset at engine start-up (Fig. 10). To minimize laser reflection from the curved contour of the inlet lip within the image background the inlet lip had to be covered with black. In absence of a black tape with aviation authorization a removable residue-free silver tape was used and painted black. To protect electronic and optic devices from dew or humidity within all casings and boxes a 25 W light bulb was installed working as a "heat ball". All necessary cables and hoses had to be secured to the ground and routed in fixed cable bridges.

Figure 12: Calibration target with checker board having an inclination angle of 6° and blackened engine inlet lip

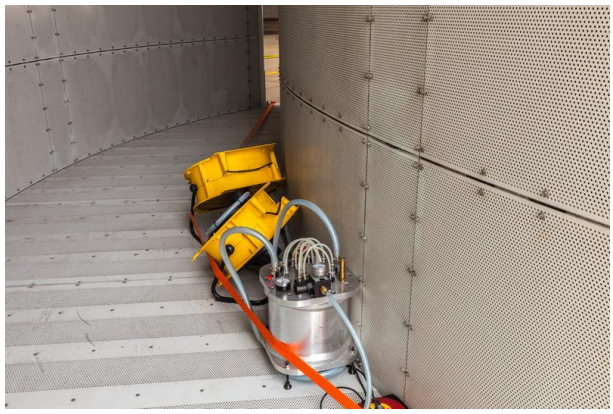

Figure 13: Particle generator and blowers between airflow guide vanes in the gate

The used type of aerosol particle generators based on Laskin nozzle principle is well known for large size wind tunnel applications, as well as the used DEHS fluid being approved via IAE consortium in advance. The pressurized air was supplied by an external mobile compressor which is located outside the hangar close to the wall to avoid any impact on the acoustic measurements running in parallel with engine jet PIV. In order to distribute the seeding particles homogeneously as possible in front of the investigated left engine, several particle generators in combination with high impulse blowers have been placed between different airflow guide vanes in the left gate fixed by tension belts and far outside of safety area within pilots view as shown in figure 13.

6. Stereo PIV Setup for Engine Jet Flow

The turbulent engine jet exhaust flow is of prominent interest for the aero- dynamic and -acoustic characterization of a real aircraft engine. Especially the development of the free shear-layer between outer flow and fan-bypass flow is an important source of high-frequency noise as well as of big interest for modeling jet flows correctly by advanced RANS methods. Unfortunately, the delivered 1/rev trigger had a jitter which was too large for precise single fan phase locking of the SPIV bypass jet flow measurements enabling a decomposition of the mean, periodic and stochastic parts of the flow velocity fields. Furthermore, the planned correlation of the instantaneous velocity fields with the respective temporally retarded acoustic pressure fluctuation signals gained from synchronized microphone array measurements need a stochastically independent input for a proper causality-correlation approach capturing all relevant acoustical frequencies emitted by the velocity (and density) fluctuations according to Lighthill's equation:

$$\partial^2\rho/\partial t^2 - a_0^2\nabla^2\rho = \partial^2 T_{ij}/\partial x_i \partial x_j, \quad T_{ij} = \rho u_i u_j + \delta_{ij}(p - a_0^2\rho). \tag{1}$$

Therefore, the SPIV measurements in the bypass jet exhaust flow have been performed at free running fan phase positions and statistically independent at 15 Hz double-image snapshot repetition rate. A *Spitlight1000* double oscillator Nd:YAG laser from *Innolas Inc*. was used as light source for the DEHS particles passing the nacelle and engine bypass. The laser system was placed at about 15 m distance from the measurement plane in a tent made of laser radiation resistant curtains while the unexpanded beam has been delivered through a long tube made of several aligned X-95 bars fixed to the ground for laser safety issues. The light sheet forming optics have been placed about 6 diameters downstream of the engine outlet in the jet axis plane within a massive steel housing fixed to the ground in order to accommodate for possible jet flow-structure interaction (see sketched set-up in figure 2 (2)). The double-cavity laser delivers approximately 450 mJ per pulse, while proper optics expanding the beam into a light sheet plane directed upstream towards the engine outlet. Two stereoscopic PIV camera configurations consisting of four sCMOS cameras from *PCO* with a resolution of 5.6 Mpx each have been arranged lateral on both sides of the V2527 engine as well in housings fixed to the concrete floor, viewing in forward scattering direction and resulting in an overlapping measurement area perpendicular to the ground and in flow direction in the immediate bypass jet exhaust flow. The size of the common measurement domain was approximately 1200 x 500 mm² in stream-

wise and wall-normal resp. radial directions. The calibration of the two stereo camera fields of view has been realized using a printed regular grid fixed between two thin glass plates for simultaneous optical access from both sides and enabling a mapping to a homogenous magnification factor of M = 4.2 px/mm for all cameras. Final alignment of each of the two stereo viewings has been achieved with sub-pixel accuracy using the disparity correction scheme on the mapped particle images implemented in *PivView3.59*. Vibrations of the camera lines-of-sight as well as of the engine position at Maximum Continuous Thrust (MCT) were below ~4 pixels amplitude corresponding to ~0.9 mm after a shift of the whole engine position of about 110 mm in upstream direction took place. The engine position has been monitored by the MODE system which enabled the calculation of the position as well as of the final thrust vector of the engine during operation. In seven MCT runs each about 2 minutes duration almost 8100 PIV images have been captured. A slight oscillation of the seeding density and the normal light sheet position occurred during the 7 runs due to the sensitivity of the seeding cloud traces to outside wind conditions and of the laser beam direction summing up along the long light way from small vibrations or density fluctuations at the laser beam.

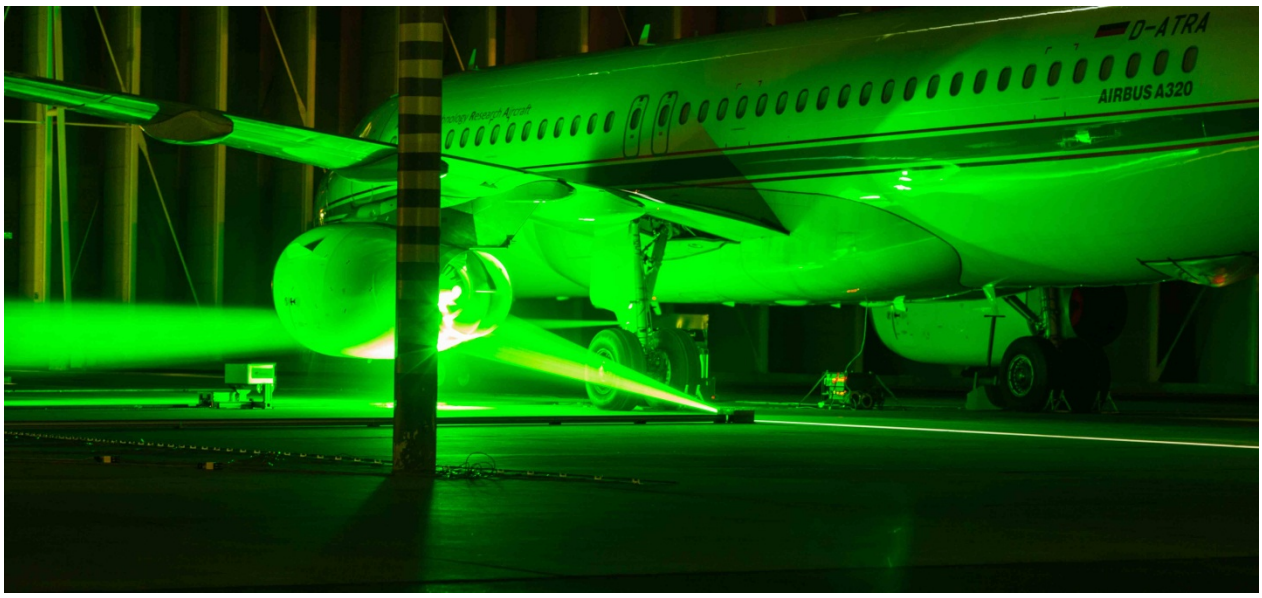

Figure 14: Laser light sheets at the ATRA V2527 engine for measuring SPIV in the engine inlet and the bypass jet exit flow during operation at MCT in the sound-attenuating hangar of the airport Hamburg

7. BOS (Background Oriented Schlieren) Setup for Engine Jet Flow

The local density gradient within the turbulent engine jet exhaust flow is another important measure for the aero- dynamic and -acoustic (see Lighthill's equation) characterization of a real aircraft engine. In order to capture the information of the projected local instantaneous density gradients in a large field of view within a relevant part of the engine jet even with time-resolution a high-speed BOS (Fig. 2 (6)) system have been installed at the A320 aircraft engine in the sound-attenuating hangar (Fig. 15 The set-up consists of four 4 Mpx high-speed cameras (*PCO Dimax*) together with eight collimated LED-arrays with approx. 9° opening angle and fast excitation electronics for pulsed light emission in the order of microseconds and a large random dot pattern on a background wall printed on retro-reflective foils fixed to a rigid x-95 bar construction close to the aircraft´s fuselage. Calibration and stitching of the four single camera views onto the jet axis area (and thus location of the density gradients) have been gained by using three checker-board calibration bars with a length of 6 m each. A total view of 4.2 m x 2 m size in x-z-direction starting at x = 3.62 m downstream of the jet exhaust with ~4200 x 2000 pixels resolution (Fig. 16) have been realized with a spatial resolution of 1.2 px/mm. The pulsed LED illumination was placed close to the camera lenses in order to achieve maximum light reflection from the retro-reflective foil in short time intervals inhibiting smearing of the local density gradients during frame acquisition. Therefore, the LEDs have been provided with pulses of electric current with 45 µs length in order to reach a saturated plateau of intense light emission after ~30 µs from which the camera frame shutter cuts out only 10 µs for illumination of the dot pattern images at $f_{\#} = 11$. At a maximum flow speed of around 300 m/s at MCT engine operation a smear of 3 mm resp. 3.6 px occurs at the measured density gradients, which is negligible with respect to the final

interrogation window size of 64 x 64 px corresponding to 53 x 53 mm². The large interrogation window has been deemed necessary in order to achieve a smooth average density gradient field. At smaller window sizes the average field was strongly biased due to strong random dot image blur in the jet core flow region (see results chapter). The BOS measurements were performed at two frame rates, one at 2 kHz and one at 200 Hz. The higher frame rate was the maximum rate of the cameras at reduced spatial resolution of 1000 x 2000 px and has been chosen for reaching temporal resolution of the convecting density gradient structures. The low frame rate was necessary for reaching statistical independence of the single snapshots enabling a proper application of the causality-correlation approach, in which the local density fluctuations and the microphone signals have to be correlated [5].

Figure 15: Retro-reflexive background with random dot pattern and four 4 Mpx *PCO Dimax* high-speed cameras with each two lateral pulsed and collimated LED-arrays

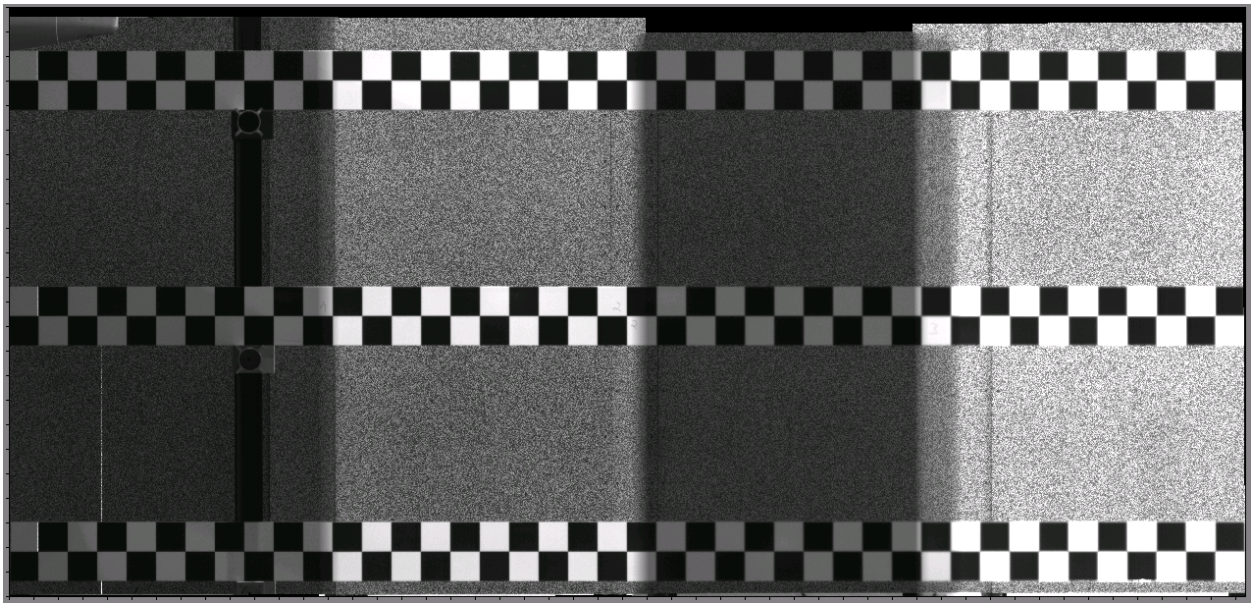

Figure 16: Stitching of the mapped four high-speed camera views each according to the checker-board calibration bars with in total ~4200 x 2000 pixels resolution at 4.2 m x 2 m-size. Middle line of calibration bar represents the jet axis

Each measurements run consists of 11,000 images, while at the low frame rate at 200 Hz a total number of 44,000 images have been captured synchronously with the microphone measurements in four separated runs. The sequences of images have been locally cross-correlated with the respective reference images of the dot pattern captured without influence of density gradients. Due to the long lines-of-sight of ~15 m from the high-speed cameras to the dot pattern on the background wall small vibrations induced from the engine in operation or from the camera chiller ended up in subpixel image shifts, which have to be corrected for each individual image before the cross-correlation scheme can be processed in a batch mode. Therefore for each camera view a small region have been used in the lower right corner in which the lines-of-sight are not affected by the density gradients in the jet flow. The local cross-correlation results with the respective reference images have been averaged in the given small domain resulting in small displacement vectors which x- and y- component is shown along a time line given by the high image frame rate of 2 kHz in figure 17. These values have been used for the correction of the measurement area of each camera and time step before stitching together all four images to one large field.

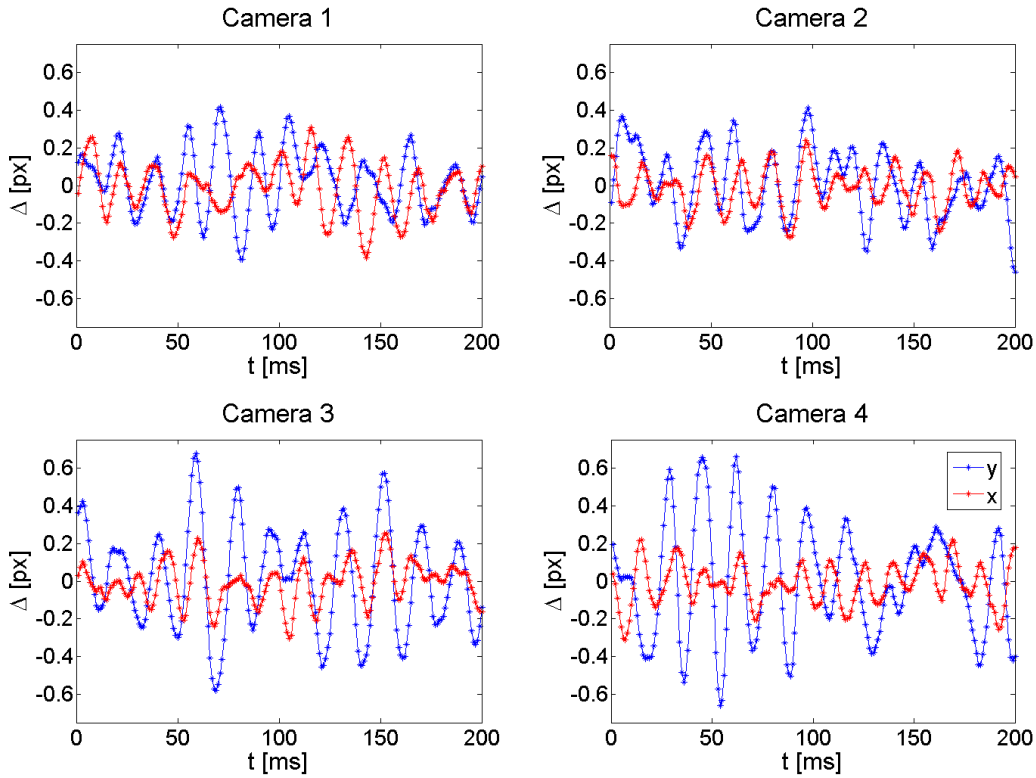

Figure 17: Time lines of vibration induced oscillations of all four camera lines-of-sight in x- and y-direction in pixels

8. PIV Post-Processing and Results

About 8000 instantaneous velocity vector fields of the SPIV measurements at the immediate engine exhaust bypass jet flow have been gained for the given field of view (Fig. 18 and 19) within 6 separate runs at MCT (~82% N1). Further SPIV measurements have been performed for one run at 75% N1 with 1000 snapshots and for two runs at 50% N1 each containing around 2100 PIV images. The evaluation has been performed with *PivView3.59* from *PivTec* with an iterative multi-grid cross-correlation scheme using image deformation with a final correlation window size of 32 x 32 px at 12 px step size according to 2.9 mm vector spacing with in total ~58,000 velocity vectors in the combined field-of-view each.

One can see small and large scale turbulent structures in the bypass flow and clearly a Kelvin-Helmholtz (KH) based instability mechanism for the development of the shear layer flow overlaid by the turbulent jet- and boundary layer flow in the instantaneous velocity vector field in figure 18 with color coded u-velocity component. The time-averaged flow field in figure 19 shows the broadening of the shear layer due to the turbulent transport mechanisms while the bypass flow itself develops to a plateau region of similar average flow velocities around 270 to 280 m/s.

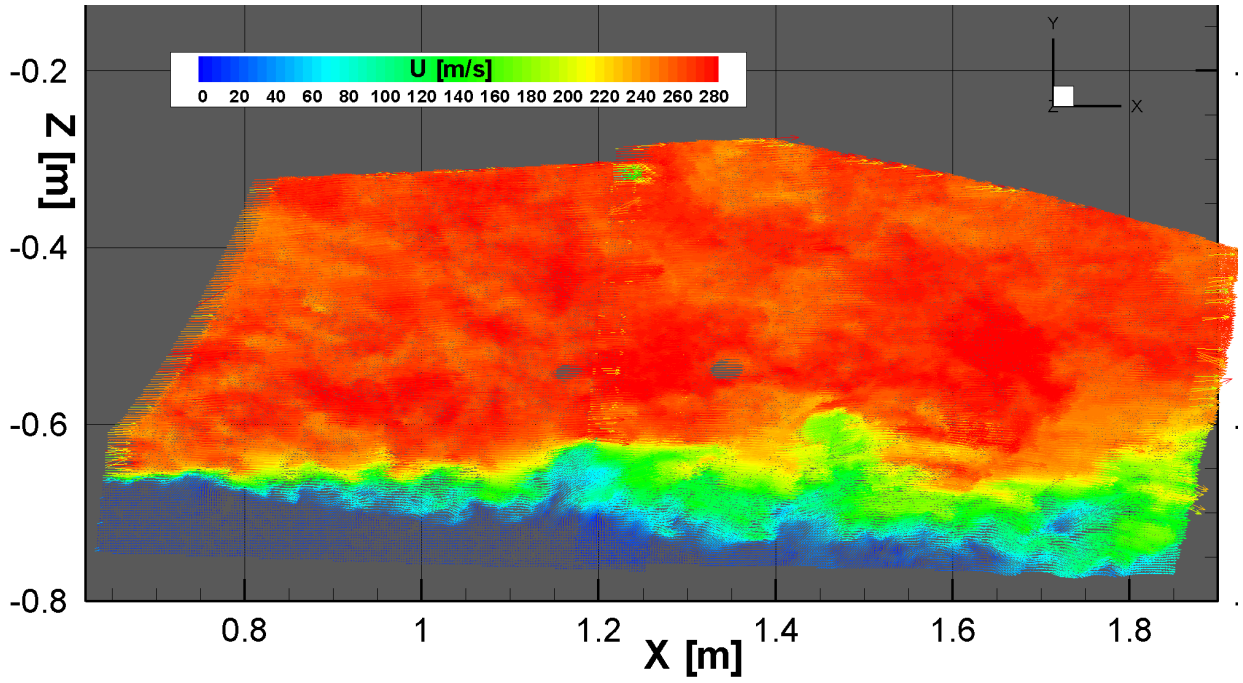

Figure 18: Instantaneous 3C- velocity vector field of the combined field of view at the bypass engine exhaust during MCT (~82% N1) with color coded u-component

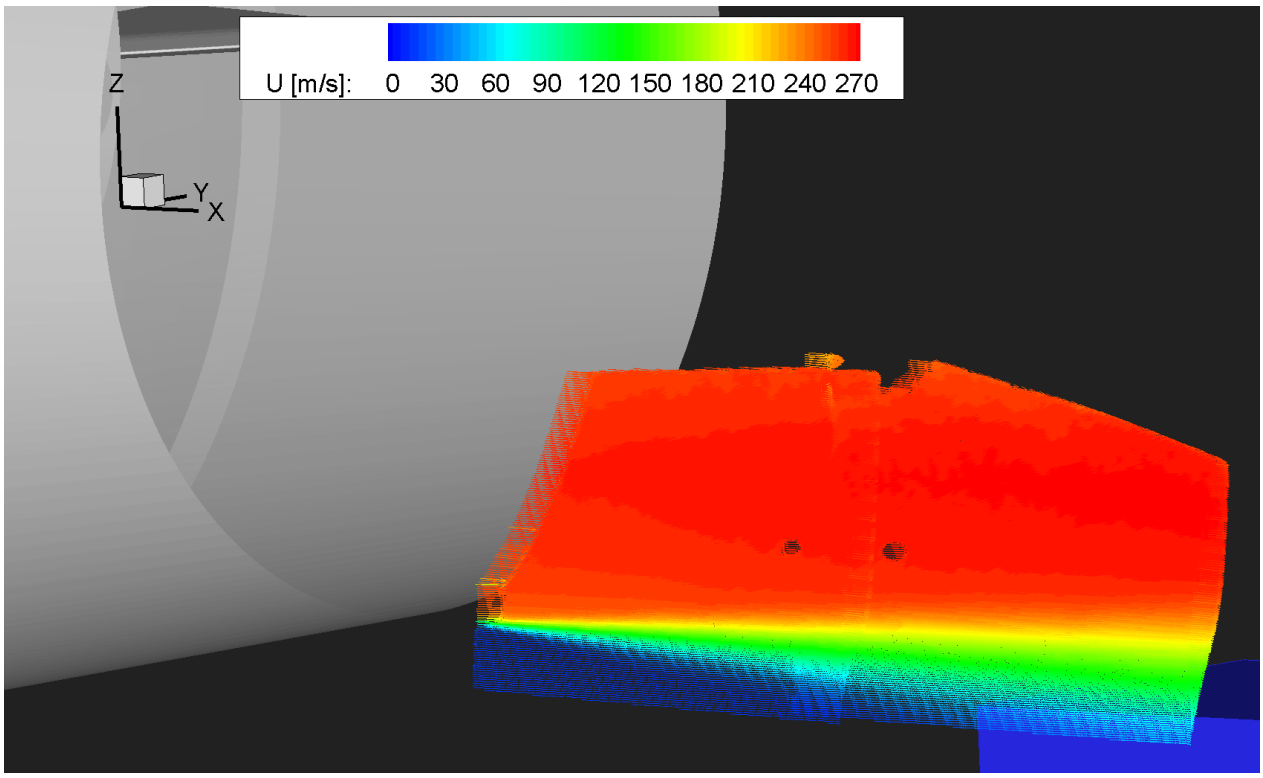

Figure 19: Averaged velocity field from one of six runs of the combined field of view at the bypass engine exhaust during MCT (~82% N1) with color coded u-component

About 1600 instantaneous velocity vector fields of the SPIV measurements at the immediate engine inlet flow have been gained (Fig. 20) within 6 separate runs at MCT (~82% N1). The evaluation has been performed with *PivView3.59* from *PivTec* with an iterative multi-grid cross-correlation scheme using image deformation using a final correlation window size of 64 x 64 px at 16 px step size according to 10 mm vector spacing with in total ~5600 vectors. The weather conditions during the measurements at the end of September with low temperatures, relatively high humidity and constant wind in the sound-attenuating

hangar, especially with the engines running, together with the laser position directly below the fuselage are not comparable to laboratory conditions required in the manual specifications. This was noticeable already during the adjustment with stopped engines but especially during the measurements with running engines by beam misalignment. The misalignment of the laser was referring mainly to the second harmonic generator, with the result of different output in light intensity for both cavities. Therefore a lot of the gained PIV double shutter images are significantly differently illuminated. Out of the 6 separate runs two are only limited evaluable. The vortex structure of the inlet vortex generates a significantly inhomogeneous distribution of the seeding, and furthermore inducing condensation of moisture due to the very low pressure region within the inlet vortex tube, resulting into light flare at the laser light sheet plane. Although the light sheet cuts only the suction tube while the major part of it is located mainly outside of the direct laser illumination, the condensation area of this hook shaped geometry leads to saturation of large areas on the CCD chip preventing PIV evaluation within these regions for many single images. On the other hand the vortex structure reduces the particle density within remote areas preventing PIV evaluation as well. Since the vortex structure in the engine inlet varies greatly with the image frequency of 5 Hz from shot to shot in its position any masking is hardly possible at reasonable efforts.

The two used PIV systems at the engine inlet and exhaust jet flow have been different in hardware due to availability and support different maximum frame rates, 5 Hz at the inlet and 15 Hz at the jet exhaust flow. In combination with the geometric arrangement in which the “jet exhaust”-PIV system from behind the engine is flashing in forward direction with reflections on the nacelles and on the ground a not considered multiple illumination of the second frame for the inlet PIV system occurred. This results in a multiple illustration of the suction tube and a blurred image of the particles in the second frame reducing the evaluation quality.

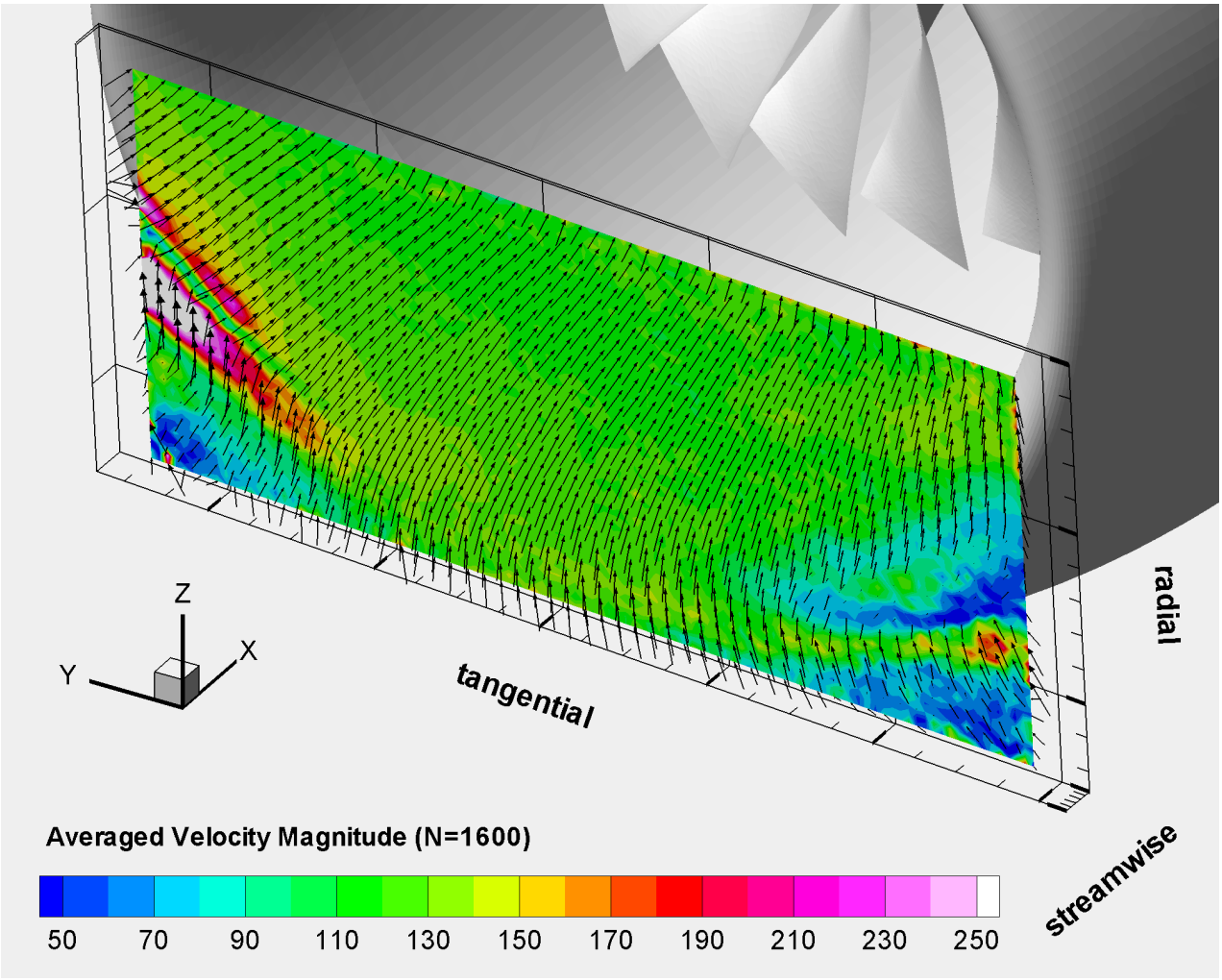

Figure 20: Averaged velocity field from six runs (N=1600 images) of the intake flow during MCT (~82 % N1) with color coded velocity magnitude of uvw-components

In summary, it can be noted that the chosen setup was successfully able to capture the inlet vortex in the selected light sheet plane, but exactly this fact leads to unexpected problems for the image evaluation. For the above mentioned reasons (fluctuation and saturation) the time averaging results in a suppression of the vortex structure visibility. Firstly, individual images with strong vortex structures could hardly be evaluated due to inhomogeneous seeding and reflections of the vortex tube (caused by condensation of moisture in the low pressure core). Secondly, in the time-averaged result the inlet vortex is suppressed due to the high fluctuation of the local occurrence. Flow fields of single images are not representative. Figure 20 shows the unspectacular time averaged vector field of the inlet flow without a no longer visible inlet vortex. The already mentioned missing masking becomes clearly visible for the still remaining and various laser reflections from vibrating nacelle with its strongly curved inlet geometry. For both lower corners of the field of view the laser energy and particle concentration was low.

9. BOS image evaluation and results

The BOS evaluation is based - like the one for SPIV - on an iterative multi-grid cross-correlation scheme using image deformation using *PivView3.59*. The BOS images are of high-quality concerning contrast and sharpness in most of the regions of the flow around the jet, while in the jet core region and around the strongest density gradients a blurring of the particle images reduces the possible spatial resolution governed by the cross-correlation window size. While the maximum local dot pattern image displacement between the reference- and the measurement image is around four pixels at the strongest density gradients most of the displacement vectors are about one to two pixels length only and in the region outside the flow even in sub-pixel range. A first evaluation using a final interrogation window size of 16 x 16 px² corresponding to 13.3 mm spatial resolution with in total 756,000 vector shows a reasonable distribution of density gradients inside and especially around the jet (Fig. 21). Even the convection of small scale events within the jet core region can be followed by eye inspection easily within the 2 kHz time-resolved displacement fields. But after averaging all instantaneous results to a mean displacement field a staggered pattern appears for such small correlation window sizes in the core regions which is caused by the blurring of the locally fixed background dot pattern resulting in systematically biased vector fields due to a lack of spatial resolution.

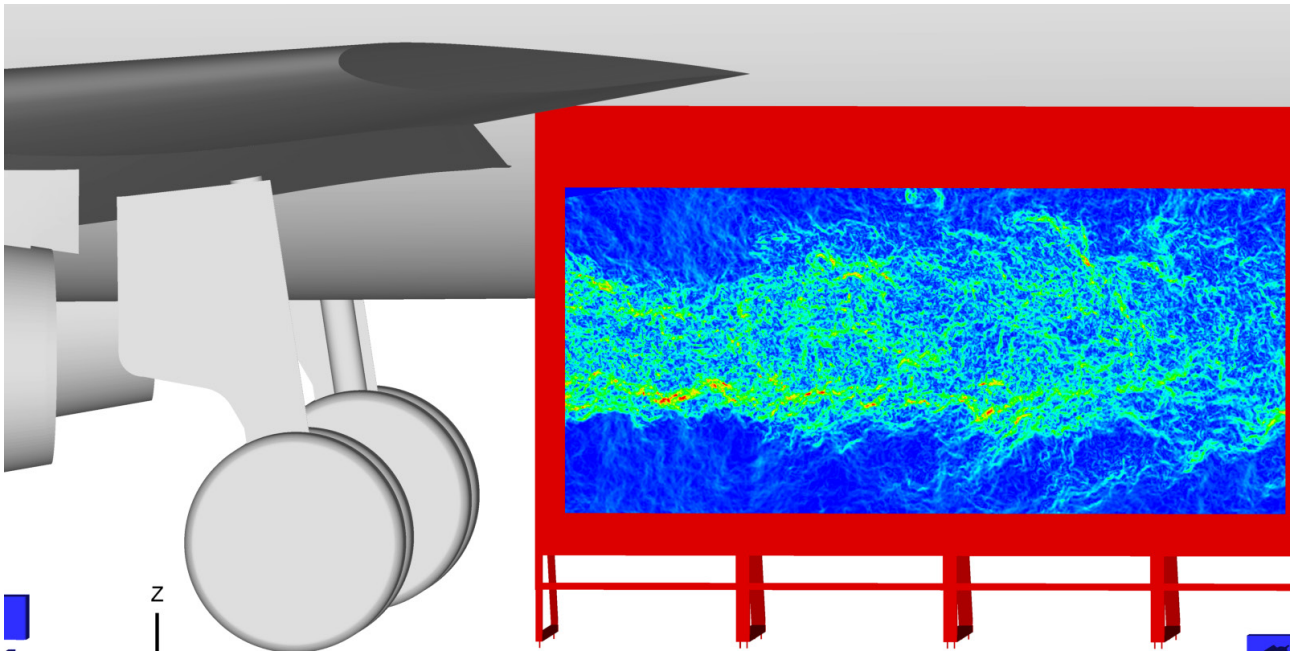

Figure 21: Instantaneous density gradient displacement contour field of the combined field of view over whole jet between 3.6 m to 7.8 m downstream of the jet exhaust during MCT (~82 % N1) (Magnitude of displacement color coded)

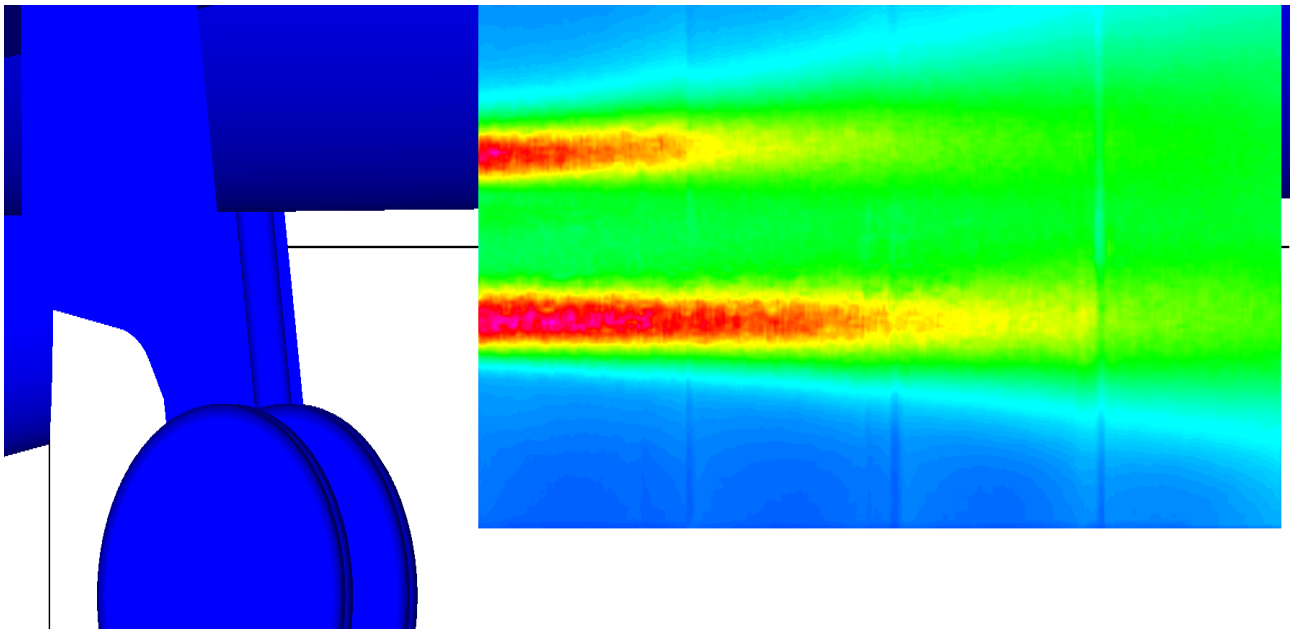

Figure 22: Averaged density gradient field from one of six runs (bottom) of the combined field of view over whole jet between 3.6 m to 7.8 m downstream of the jet exhaust during MCT (~82 % N1) (Magnitude of displacement color coded)

Therefore and due to the plan using the results for a decent (unbiased) causality-correlation of the measured density gradient fluctuations with the microphone signals a relatively large final interrogation window size of 64 x 64 px² has been used corresponding to 53 mm spatial resolution in each direction in order to accommodate for the systematic blurring issue. This reduction in spatial resolution on a 4.2 x 2 m² field still enables us a visualization of the main energy containing flow structures carrying density gradients in this multi-scale free turbulent jet flow field on the basis of 47,250 vectors for each time step of 44,000 independent snapshots and two series of in total 22,000 time-resolved images. In comparison to the noise emitted at the shear layer measured by SPIV in the immediate jet exhaust region the present large area further downstream measured by BOS is known to be an origin of broad-banded lower frequency noise, so that we cannot expect a strong under-sampling of the relevant noise emitting structures connected to the measured density gradient fluctuations.

The average density gradient field shows that due to interaction of the installed jet with the wing, flap and pylon rotational symmetry is broken (Fig. 22). Nevertheless, a tomographic reconstruction of the average density field by the Fourier back projection method shall offer us the possibility to deduce the 3D temperature field as we know the distribution of the single gaseous species from 1D simulation.

10. Summary

Within a one week measurement campaign all envisaged measurement techniques (IPCT/PROPAC, two SPIV systems for jet and intake flow, MODE, BOS and acoustic array) have been applied successfully in order to quantify several important measures of the left IAE-V2527 engine flow of DLR's Advanced Technology Research Aircraft A320-ATRA in ground operation up to maximum continuous thrust (MCT) in the sound-attenuating hangar at airport Hamburg. With respect to the operation conditions the gained data are of high quality and will be used in coupling to each other as well as to results of advanced numerical methods to enhance the understanding of the engine flow physics in terms of aero-dynamics, -elastics and acoustics. Despite the time limitations and overall challenging large-scale conditions no total failure of single components occurs although individual parameters had to be adjusted on site. The administrative expense in advance was quite extensive due to certification processes and laser safety issues have been underestimated during project planning. Detailed analyzes of the extensive measurement data in terms of noise source investigations and of comparisons with and validation of accompanying numerical simulations will be discussed in further publications.

Acknowledgements

The support from LHT to the DLR project SAMURAI confirmed the good relationship based on closely co-operations in research on aircraft noise sources during many years. For the ground test on ATRA a variety of DLR staff has been involved, which goes far beyond the list of authors. Overall 51 DLR employees have been registered for the week-long measurement at the airport and even more have been involved in preparation process.

References

[1] Online document: Schröder A. (2012) SAMURAI project sketch, DLR, retrieved from http://www.dlr.de/as/en/desktopdefault.aspx/tabid-183/251_read-33607/
[2] Online document: Dambowsky F., DLR news, retrieved from http://www.dlr.de/dlr/en/desktopdefault.aspx/tabid-10081/151_read-8278/year-all/#gallery/12408
[3] Online document: Schmidt A., Hamburg Airport, Zentralbereich Umwelt, retrieved from http://www.airport.de/de/u_umwelt_laermschutzhalle.html
[4] Flight Test Requirement, SAMURAI - Non-invasive Ground Testing of ATRA Engine V2527, Doc.-No.: FTR-659-SMH-16362-13-021
[5] Henning, Arne und Koop, Lars und Schröder, Andreas (2013) Causality correlation analysis on a cold jet by means of simultaneous particle image velocimetry and microphone measurements. Journal of Sound and Vibration, Vol. 332, Seiten 3148-3162. ELSEVIER. DOI: 10.1016/j.jsv2013.01.027. ISSN 0022-460X
[6] Richard, H. & Raffel, M. (2001) Principle and applications of the background oriented schlieren (BOS) method. *Measurement Science and Technology*. 12 (9), 1576-1585

Abbreviations

ACARE:	Advisory Council for Aviation Research and Innovation in Europe
ATRA:	Advanced Technology Research Aircraft
BOS:	Background Oriented Schlieren
CAA:	Computational Aeroacoustics
CCD:	Charge Coupled Device
CFD:	Computational Fluid Dynamics
CSM:	Computational Structural Mechanics
DAQ:	Data Acquisition
DES:	Detached-Eddy Simulation
DEHS:	Dioctyl sebacate
DLR:	Deutsches Zentrum für Luft- und Raumfahrt
DNS:	Direct Numerical Simulation
FTI:	Flight Test Instrumentation
FTR:	Flight Test Request
IAE:	International Aero Engine
ICAO:	International Civil Aviation Organization
IPCT:	In-Plane Pattern Correlation Technique
IRT:	Infrared Thermography
LAN:	Local Area Network
LED:	Light Emitting Diode
LES:	Large Eddy Simulation
LHT:	Lufthansa Technik
MCT:	Maximum Continuous Thrust
MODE:	Marker-Based Optical Deformation Measurement
Nd:YAG:	Neodymium-doped Yttrium Aluminum Garnet
PIV:	Particle Image Velocimetry
PROPAC:	Projected Pattern Deformation Correlation Technique
PSP:	Pressure Sensitive Paint
RANS:	Reynolds-Averaged Navier-Stokes
RAID:	Redundant Array of Independent Disks
ROI:	Region of Interest
SAMURAI:	Synergy of Advanced Measurement techniques for Unsteady and high Reynolds number Aerodynamic Investigations
sCMOS:	Scientific Complementary Metal–Oxide–Semiconductor
SPIV:	Stereoscopic Particle Image Velocimetry
TOGA:	Take-off and Go Around
TSP:	Temperature Sensitive Paint
UHBR:	Ultra High Bypass Ratio test rig
URANS:	Unsteady Reynolds-Averaged Navier-Stokes